Ordinary and extraordinary phonons and photons: Raman study of anisotropy effects in the polar modes of $MnGa_2Se_4$

P. Alonso-Gutiérrez and M. L. Sanjuán*

Instituto de Ciencia de Materiales de Aragón (Universidad de Zaragoza-CSIC), Facultad de Ciencias, Universidad de Zaragoza, 50009 Zaragoza, Spain

(Received 1 April 2008; revised manuscript received 27 May 2008; published 29 July 2008)

We present a spectroscopic study of optovibrational properties of $MnGa_2Se_4$, an ordered-vacancy compound with defect chalcopyrite structure and uniaxial optical behavior. Anisotropy affects the Raman spectrum of noncentrosymmetric media in two different ways: for nonpolar modes, birefringence produces a dephasing between ordinary and extraordinary waves that results in an apparent violation of selection rules. In polar modes, in addition, anisotropy affects phonon propagation, resulting in the phenomenon of directional dispersion. The Raman spectrum of $MnGa_2Se_4$ single crystals is measured onto three different crystallographic planes as a function of the polarization direction of incident and scattered light. Loudon equations are used to assign the symmetry and character of each mode. Two different regimes are found: For low-frequency modes, polarity is weaker than anisotropy effects and these modes show negligible directional dispersion. On the contrary, for high-frequency modes, anisotropy effects are negligible and these modes behave as quasicubic ones. By analyzing the intensities of the polar modes, information concerning the electron-phonon mechanisms involved in the activity of polar modes is obtained. The relative magnitude of electro-optic to deformation potential mechanisms participating in LO modes is derived.

DOI: 10.1103/PhysRevB.78.045212 PACS number(s): 78.30.Fs, 63.20.kg, 42.65.−k, 78.20.Fm

I. INTRODUCTION

Due to their noncentrosymmetric structure and high polarizability, tetrahedral semiconductors have been widely investigated in the search of nonlinear optical (NLO) properties.[1] Ternary chalcopyritelike compounds are especially interesting since their structural and optical anisotropy provides the additional possibility of achieving phase-matching condition.[2–4] Ordered vacancy compounds (OVC) of AB_2C_4 type are also promising candidates for applications based on NLO properties. Among them, $HgGa_2S_4$, $CdGa_2S_4$, and their derivatives, with a defect chalcopyrite structure, are the most studied materials.[5–8]

Raman spectroscopy has been widely used to study the fundamental physics of zincblendelike semiconductors. In connection with NLO, light scattering yields information on the electron-phonon interactions involved in the activity of the longitudinal component of polar phonons, specifically the electro-optic mechanism.[9,10] In anisotropic materials, uniaxial optical behavior affects the propagation of photons and phonons, thus Raman scattering can be used to study such properties. In nonpolar modes, the uniaxial character affects only light propagation and results in an apparent loss of polarization rules. In polar modes, both phonon and photon propagation are affected by structural anisotropy. Then, in addition to light depolarization, the well-known phenomenon of directional dispersion occurs, according to which the frequency of polar modes depends not only on the relative directions of phonon polarization and propagation but also of those with respect to the optic axis. In his classical work of 1964,[11] Loudon developed a formalism to describe the properties of long-wavelength lattice vibrations in uniaxial media and gave expressions for the dependence of the phonon frequencies and intensities on geometrical configuration. Loudon, however, did not consider light depolarization within the sample due to the anisotropy of refraction indices. An adequate treatment of this effect must be included for a correct understanding of the vibrational properties in anisotropic media.

Loudon's equations have been widely used in the literature, for example in binary wurtzite-type compounds[12,13] or others such as lithium niobate.[14] A study of polar modes in the defect chalcopyrite compounds $CdGa_2Se_4$ (Ref. 15), $CdGa_2S_4$ (Ref. 16), $CdAl_2S_4$, and $CdAl_2Se_4$ (Ref. 17) following Loudon's model has also been reported. In these studies, interest is usually focused only on directional dispersion of phonon frequencies rather than on Raman intensities.

In this paper we present a Raman study of uniaxial effects in the polar modes of $MnGa_2Se_4$, an OVC with defect chalcopyrite structure and $I\bar{4}$ space group.[18] In OVC, cation asymmetry and crystallographically ordered vacancies lead to a tetragonal structure with unit cell doubled with respect to its parental cubic zincblende compounds and $c \leq 2a$. For $MnGa_2Se_4$, $a=5.677[1]$Å and $c=10.761[2]$Å (Ref. 19). The doubling of the unit cell causes structural and optical anisotropy; as in their related chalcopyrite compounds, optical birefringence is expected.

According to factor group analysis, 13 Raman active modes are expected in $MnGa_2Se_4$, divided in $3A+5B+5E$, where A modes are nonpolar, and B and E modes are polar. Normal coordinates of these modes can be found in Ref. 20. In a previous work, concerning the Raman study of the $Zn_{1-x}Mn_xGa_2Se_4$ series, a preliminary assignment of mode symmetry for $MnGa_2Se_4$ was made.[21] In a subsequent work,[22] we studied the influence of optical anisotropy in the selection rules of the nonpolar modes of $MnGa_2Se_4$. We determined the phase difference between the ordinary and extraordinary waves and the parameters of the Raman tensors of the three A modes, and we also proposed a method to estimate the birefringence from Raman measurements.

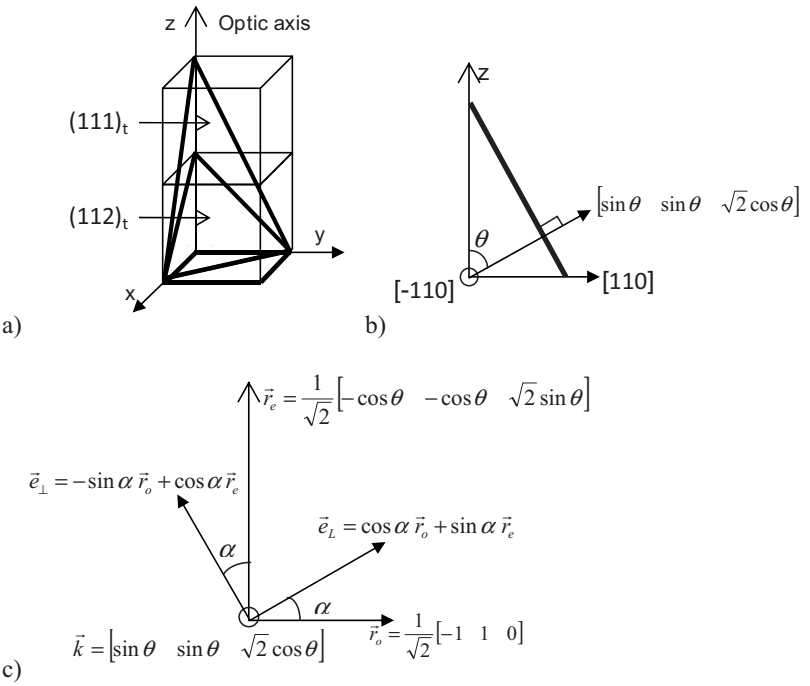

FIG. 1. (a) Schematic picture of $MnGa_2Se_4$ unit cell, showing the $(001)_t$, $(112)_t$, and $(111)_t$ tetragonal planes where measurements have been performed. In the cubic reference system used in this work, these planes have indices (001), (111), and $(11\frac{1}{2})$, respectively. (b) Reference system used to define the direction of propagation of light and the angle θ between the optic axis and the normal to the plane. (c) Reference system and axes used to define the direction of polarization of light.

In this work we present an experimental and theoretical study of the polar modes of $MnGa_2Se_4$. Since the effect of optical anisotropy in incident and scattered light has been explained in the previous work,[22] we focus this paper on the influence of anisotropy in the symmetry and intensity of the polar modes.

II. EXPERIMENT DETAILS

Small single crystals of $MnGa_2Se_4$ were grown by the chemical vapor transport method using iodine as transport agent.[23] Structural,[24] optical,[25] and Raman[21,22,26,27] characterization of our samples can be found in previous works. Raman spectra were collected in a Dilor XY spectrometer with a liquid-nitrogen cooled CCD detector. The experiments were performed in backscattering geometry. Laser light at 514.53 nm was focused on the sample through an X50 microscope objective lens, the power at the sample being of ~ 1 mW. Spectral resolution was better than 3 cm^{-1}. The Si mode at 520 cm^{-1} and the well established frequencies of the nonpolar A modes have been used for frequency calibration.

III. EXPERIMENT RESULTS

The small size of $MnGa_2Se_4$ crystals (2 mm maximum dimension) did not allow us to cut them in selected planes, so our study is limited to natural growth planes, the most frequent of which is the $(112)_t$ tetragonal face. Some crystals presenting the $(001)_t$ and $(111)_t$ planes were also found. For convenience, we shall use in the following a pseudocubic reference system in which the Miller indices corresponding to the tetragonal $(112)_t$ and $(111)_t$ planes are $(111)_c$ and $(11\frac{1}{2})_c$, respectively. These planes are schematically depicted in Fig. 1(a). Cubic subscripts will be omitted for simplicity. Thus, our experiments have been performed on three crystallographic planes: (001), (111), and $(11\frac{1}{2})$. We denote as θ the angle formed by the optic axis and the plane normal, which is also, in our backscattering experiments, the direction of incident and scattered light. For the three planes under study $\theta=0°$, 54.74°, and 70.53°, respectively (see Fig. 1).

Within each plane, Raman spectra were measured as a function of α, the angle formed by the electric field of the incident light and the [−110] crystal direction, which is common to the three planes. To change α, the sample was rotated about the normal to the surface. For each sample position, two spectra were recorded, with incident and scattered light polarization either parallel or perpendicular to each other. The spectral intensities in such configurations will be denoted as $I_\parallel(\alpha)$ and $I_\perp(\alpha)$, respectively.

Figure 2 shows the frequencies of the polar modes as a function of θ. The three totally symmetric A modes, at ω

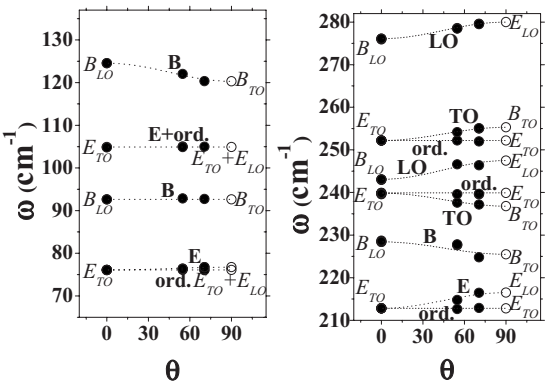

FIG. 2. Raman shifts of the (left) low- and (right) high-frequency polar modes as a function of the angle formed by the phonon propagation direction and the optic axis. Solid dots are experimental data. Dashed lines are fits to the frequency expressions (2a) and (2b) or (3a) and (3b). Open dots represent the LO and TO frequencies at $\theta=90°$ derived from the fit.

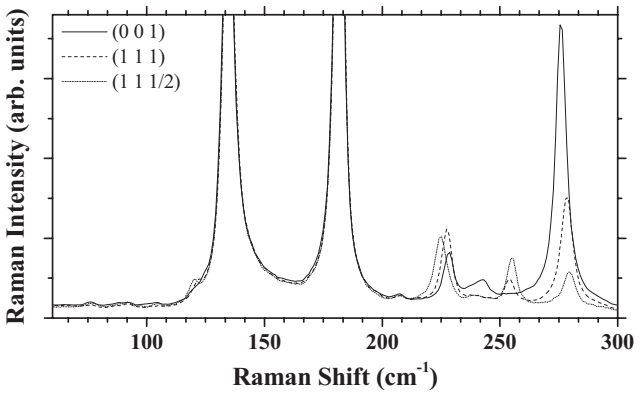

FIG. 3. Raman spectra in parallel configuration along the [−110] direction, recorded on (001), (111), and $(11\frac{1}{2})$ planes.

=134.7, 181.8, and 207.5 cm^{-1}, were studied in Ref. 22 and are omitted here for convenience. As shown in Fig. 2, some modes show strong directional dispersion, whereas others have an almost constant frequency. This behavior is exemplified in Fig. 3, which shows the spectrum measured along the [−110] direction in three different crystallographic planes. Except for obvious cases, the symmetry and character of each peak can only be determined by measuring the angular dependence of Raman intensities within each plane. As an example, we plot in Fig. 4 the intensities $I_{\parallel}(\alpha)$ and $I_{\perp}(\alpha)$ of the polar modes in the plane $(11\frac{1}{2})$. We call this kind of plots rotational diagrams.

IV. MODEL AND DISCUSSION

A. Frequencies of the polar modes

Mode polarity in uniaxial media is combined with anisotropy derived effects, resulting in directional dispersion of frequencies and the creation of mixed-symmetry or mixed-character modes. Loudon formalism[11] is used to explain the behavior of polar modes in uniaxial media. For a polar mode, two different LO and TO frequencies are *a priori* expected, according to whether the phonon polarization and propagation directions are parallel or perpendicular to each other, respectively. In backscattering geometry, longitudinal modes are polarized in a direction parallel to the incident light, and transverse modes are polarized in directions perpendicular to the incident light. Phonon polarizations are known from Raman tensor tables.[11]

In uniaxial media one must also consider the orientation of phonon polarization and propagation relative to the optic axis. Thus, for each cubic or pseudocubic polar mode, four characteristic frequencies are defined: $\omega_L^{\parallel}$, $\omega_L^{\perp}$, $\omega_T^{\parallel}$, and $\omega_T^{\perp}$, where L and T denote longitudinal and transverse character, and $\parallel$ and $\perp$ denote phonon polarization parallel and perpendicular to optic axis, respectively. For the $\bar{4}$ point group of $MnGa_2Se_4$, $\parallel$ corresponds to B modes and $\perp$ to E modes. For clarity, we rewrite the characteristic frequencies as $B_{\mathrm{LO}}=\omega_L^{\parallel}$; $B_{\mathrm{TO}}=\omega_T^{\parallel}$; $E_{\mathrm{LO}}=\omega_L^{\perp}$; and $E_{\mathrm{TO}}=\omega_T^{\perp}$.

The same as light, phonons in uniaxial media can be divided into two components. When phonon polarization is perpendicular to its propagation, and also to the optic axis, it is called an ordinary phonon, and its frequency does not depend on θ. Only E_{TO} modes fulfill these conditions. In all other cases, phonons are called extraordinary and their frequencies depend on the relative directions explained above and on the four characteristic frequencies. The frequencies of the extraordinary phonons are solutions of the equation,[11]

$$\varepsilon_{\parallel}\left[\frac{B_{\mathrm{LO}}^2-\omega^2}{B_{\mathrm{TO}}^2-\omega^2}\right]\cos^2\theta+\varepsilon_{\perp}\left[\frac{E_{\mathrm{LO}}^2-\omega^2}{E_{\mathrm{TO}}^2-\omega^2}\right]\sin^2\theta=0, \quad (1)$$

with $\varepsilon_{\parallel}$ and $\varepsilon_{\perp}$ being the components of the dielectric tensor in the directions parallel and perpendicular to optic axis, respectively. Equation (1) is quadratic in ω so it has two solutions. Following Loudon,[11] it is convenient to discuss two limiting situations, which are present in many crystals:

(i) In modes with strong polar character, $|\mathrm{LO\text{-}TO}| \gg |B\text{-}E|$ and the solutions for extraordinary phonons are given by:

$$\omega^2=B_{\mathrm{LO}}^2\cos^2\theta+E_{\mathrm{LO}}^2\sin^2\theta \quad \text{quasilongitudinal extraordinary mode,} \quad (2a)$$

$$\omega^2=B_{\mathrm{TO}}^2\sin^2\theta+E_{\mathrm{LO}}^2\cos^2\theta \quad \text{quasitransverse extraordinary mode.} \quad (2b)$$

These expressions correspond to modes with mixed B and E symmetry; the mixing depends on the phonon propagation direction. Only in high-symmetry planes (θ=0, θ=90) do the modes have pure B or E symmetry. We shall use the notation $\widetilde{\mathrm{LO}}$ and $\widetilde{\mathrm{TO}}$ for the quasilongitudinal and quasitransverse extraordinary modes, respectively. This situation corresponds to the isotropic or quasicubic limit.

(ii) In the opposite limit, when mode polarity is weak, $|\mathrm{LO\text{-}TO}| \ll |B\text{-}E|$, and solutions of Eq. (1) are modes with polarization parallel or perpendicular to the optic axis

$$\omega^2=B_{\mathrm{TO}}^2\sin^2\theta+B_{\mathrm{LO}}^2\cos^2\theta \quad \text{extraordinary } B \text{ mode,} \quad (3a)$$

$$\omega^2=E_{\mathrm{TO}}^2\cos^2\theta+E_{\mathrm{LO}}^2\sin^2\theta \quad \text{extraordinary } E \text{ mode.} \quad (3b)$$

We shall use the notation $\widetilde{B}$ and $\widetilde{E}$ for the extraordinary B and E modes, respectively.

Expressions (2a), (2b), (3a), and (3b) can be used to fit the dependence of the peak frequencies on propagation direction, shown in Fig. 2. For that purpose, we previously have to assign the B, E, LO, or TO character to each of the observed modes. In some cases, the assignment is straightforward: in the (001) plane, only B_{LO} modes are active, besides A modes; E_{TO} modes, although allowed by symmetry in this plane, yield zero intensity by tensor selection rules. B_{TO} and E_{LO} modes would be detected for θ=90 but the (110) plane is not available. Thus, the assignment has been made based on the examination of the angular dependence of the peak intensities within each plane (rotational diagrams), for which Loudon equations *for the intensities* have to be used. This study will be presented in the following section. Here we only use the result of such treatment. In that way, we find

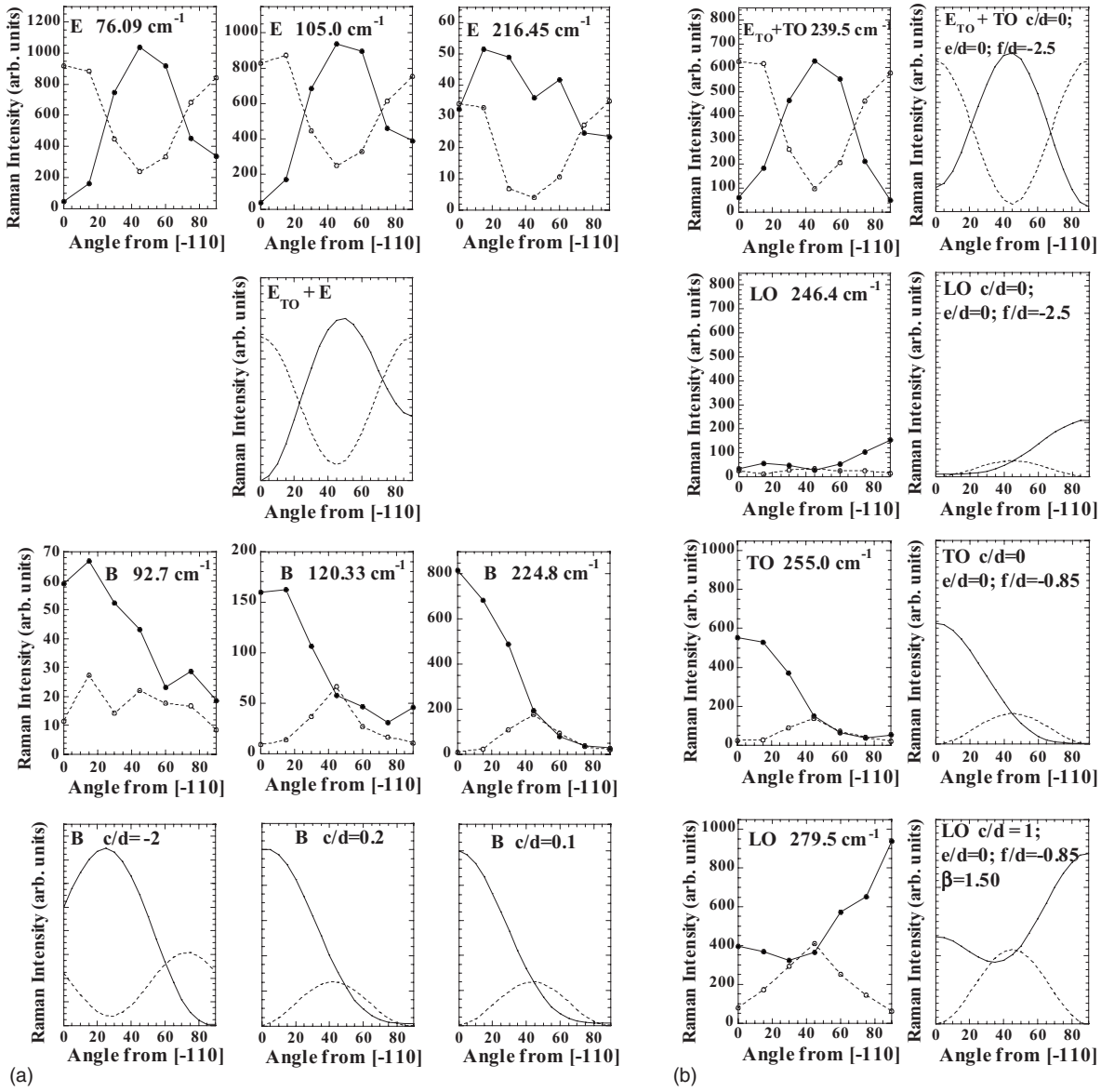

FIG. 4. Rotational diagrams in $(11\frac{1}{2})$ plane for (a) B and E modes at low frequency, where the anisotropic forces predominate over polar forces, and (b) high-frequency longitudinal and transverse modes, where polar character predominates over anisotropy. Experimental data are represented by solid ($I_{\parallel}$) and white ($I_{\perp}$) dots joined by lines as an eye guide. Plots without dots show the intensities calculated using Eqs. (12a), (12b), (13a), and (13b) for $\tilde{B}$ and $\tilde{E}$ quasimodes, respectively, and Eqs. (16a), (16b), (17a), and (17b) for $\widetilde{\mathrm{LO}}$ and $\widetilde{\mathrm{TO}}$ modes, respectively, with tensor parameters indicated in Table II and dephasing parameter for this plane. In part (b), each LO-TO pair of modes are plotted in the same intensity scale, to emphasize the effect of dipolar field on the longitudinal modes.

that the high-frequency modes (above 230 cm^{-1}) have very small tetragonal splittings and are assigned to $\widetilde{\mathrm{LO}}$ and $\widetilde{\mathrm{TO}}$ modes of situation (i), while low-frequency modes fulfill situation (ii) and they are attributed to $\tilde{B}$ or $\tilde{E}$ quasimodes. This procedure also allows us to identify the five ordinary E_{TO} phonons among the modes whose frequencies do not change as a function of θ. Frequencies of ordinary phonons coincide in the (001) plane with $\widetilde{\mathrm{TO}}$ extraordinary phonons. Although in this plane E modes are forbidden, they are detected weakly due to polarization leakage.

We show in Table I the assignment of the observed peaks and the characteristic frequencies used to fit the data to Eqs. (2a), (2b), (3a), and (3b). For completeness, nonpolar modes are also included.

Mode polarity is found to increase as frequency increases. For low-frequency modes, the LO-TO splitting is negligible or smaller than a few cm^{-1}, whereas for the highest-frequency pair the B_{LO}-B_{TO} splitting is higher than 20 cm^{-1}, and that between E_{LO} and E_{TO} is of 28 cm^{-1}.

The polar splitting of $MnGa_2Se_4$ can be compared to those of related zincblende or chalcopyrite compounds. In general terms, the splitting increases along the chalcogenide sequence Te, Se, S, O, and is also higher for zincblende than for chalcopyrite compounds. Some examples are given: 75 cm^{-1} for ZnS (Ref. 28), 64 cm^{-1} for CdS (Ref. 13),

TABLE I. Mode assignment in $MnGa_2Se_4$. Columns two to four show the experimental frequencies in (001), (111), and $(11\frac{1}{2})$ planes, respectively. Last column shows the frequencies used, together with those obtained in the (001) plane, to fit the experimental data to Eqs. (2a), (2b), (3a), and (3b). The five $B+E$ pairs of modes are separated by horizontal lines. For completeness, the three A modes are included. Their frequency is independent of θ.

Assignment	Expt. freq. (001)	Expt. freq. (111)	Expt. freq $(11\frac{1}{2})$	Fitted freq. (110)
$\widetilde{\text{LO}}$	B_{LO}=276.1	278.4	279.5	E_{LO}=280.0
$\widetilde{\text{TO}}$	E_{TO}=252.2	254.1	255.0	B_{TO}=255.3
E ord.	E_{TO}=252.2	252.2	252.2	E_{TO}=252.2
$\widetilde{\text{LO}}$	B_{LO}=243.1	246.6	246.4	E_{LO}=247.5
$\widetilde{\text{TO}}$	E_{TO}=239.9	237.6	237.1	B_{TO}=236.80
E ord.	E_{TO}=239.9	239.9	239.9	E_{TO}=239.9
$\tilde{B}$	B_{LO}=228.4	227.8	224.8	B_{TO}=225.5
$\tilde{E}$	E_{TO}=212.8	214.7	216.4	E_{LO}=216.5
E ord.	E_{TO}=212.8	212.7	212.9	E_{TO}=212.8
$\tilde{B}$	B_{LO}=124.6	122.0	120.3	B_{TO}=120.3
$\tilde{E}+E$ ord.	E_{TO}=104.9	105.0	105.0	E=104.9
$\tilde{B}$	B_{LO}=92.7	92.8	92.7	B_{TO}=92.7
$\tilde{E}$	E_{TO}=76.1	76.3	76.7	E_{LO}=76.75
E ord.	E_{TO}=76.1	76.1	76.1	E_{TO}=76.1
A	134.7			
A	181.8			
A	207.5			

40 cm^{-1} for ZnSe (Ref. 29), ≈30 cm^{-1} for $CuGaS_2$ (Ref. 30), and ≈20 cm^{-1} for $CuGaSe_2$ (Ref. 31). For the defect chalcopyrite $CdGa_2Se_4$, closely related to $MnGa_2Se_4$ as regards structure and lattice parameters, the splitting is 18 cm^{-1} (Ref. 15). As expected, much higher values are found for oxides, such as wurtzite ZnO (180–200 cm^{-1}) (Ref. 13), BeO (370–400 cm^{-1}) (Ref. 13), or quartz (160 cm^{-1}) (Ref. 32). Thus, the order of magnitude of the splitting in $MnGa_2Se_4$ is close to those of compounds of similar structure and composition.

We can use the frequencies of Table I to obtain a relation between static and optic dielectric constants using generalized Lyddane-Sachs-Teller relations for uniaxial media:[33]

$$\frac{\varepsilon_{\parallel}(0)}{\varepsilon_{\parallel}(\infty)} = \prod_i \left(\frac{\omega_{\text{Li}}^{\parallel}}{\omega_{\text{Ti}}^{\parallel}}\right)^2 \quad \text{and} \quad \frac{\varepsilon_{\perp}(0)}{\varepsilon_{\perp}(\infty)} = \prod_i \left(\frac{\omega_{\text{Li}}^{\perp}}{\omega_{\text{Ti}}^{\perp}}\right)^2, \tag{4}$$

where the products in i are along all polar modes. Substituting the frequencies given in Table I, we find $\varepsilon_{\parallel}(0)/\varepsilon_{\parallel}(\infty)=1.3557$ and $\varepsilon_{\perp}(0)/\varepsilon_{\perp}(\infty)=1.3823$. These values are similar to those of $CdGa_2Se_4$: 1.45 and 1.35 for parallel and perpendicular components, respectively.[15]

B. Intensity of polar modes

In anisotropic media, birefringence produces a dephasing between the ordinary and extraordinary components of light, which results in a change in polarization of incident and scattered light. In nonpolar modes this yields the apparent violation of Raman selection rules, but the Raman intensity is still given by the usual expression,

$$I = C\left|\sum_{i,j=x,y,z} e_s^i R_{ij} e_L^j\right|^2,$$

where R_{ij} are the components of the Raman tensor and $\boldsymbol{e_L}$ and $\boldsymbol{e_s}$ are the polarization directions of the electric field associated with incident and scattered light, respectively. C is a proportionality factor. For polar modes, the dependence of the Raman tensors on the phonon polarization and propagation directions has to be taken into account together with light depolarization. Loudon formalism gives a generalization of the expression for the Raman intensity as

$$I = C\left|\sum_{i,j,k=x,y,z} e_s^i R_{ij}^k (\xi^k + \beta\kappa^k) e_L^j\right|^2, \tag{5}$$

where $\boldsymbol{\xi}$ and $\boldsymbol{\kappa}$ represent the phonon polarization and propagation directions, respectively. The parameter β is proportional to the dipolar electric field along $\boldsymbol{q}_{\text{LO}}$ created by the ions.[34] Index k in the Raman tensor indicates the polarization of the corresponding vibration. Optical anisotropy was treated in Ref. 22 for nonpolar modes, but it applies as well to polar phonons. A brief reminder is given now.

1. Influence of anisotropy in incident and scattered light

Light propagating in uniaxial media is divided into two components:[35] ordinary wave, whose polarization is always perpendicular to the optic axis and to the direction of propagation of light, which propagates with a refraction index n_o; and extraordinary wave, whose refraction index n_{eff} varies with the direction of propagation relative to the optic axis, in the form $1/n_{\text{eff}}^2=(\cos\theta/n_o)^2+(\sin\theta/n_e)^2$, n_e being the extraordinary refraction index and θ the angle defined above. Due to the difference of refraction indices, a phase difference is produced between the two waves, given by

$$\delta = \frac{2\pi}{\lambda}(n_{\text{eff}} - n_0)d, \tag{6}$$

where d is the path that the light runs through the medium and λ is the wavelength. The difference $\Delta=n_{\text{eff}}-n_o$ is the birefringence of the material.

To account for dephasing effects in the calculation of Raman intensities with Eq. (5), we extract from the polarization vectors of incident and scattered light the component perpendicular to the optic axis, which is the ordinary wave, the remaining part corresponding to the extraordinary wave. The dephasing is introduced by multiplying the ordinary component by a factor $e^{i\delta}$. So, as incident light goes through the medium, its polarization vector is changed from $\vec{e}_L = \cos\alpha\vec{r}_o + \sin\alpha\vec{r}_e$ to $\vec{e}'_L = \cos\alpha e^{i\delta}\vec{r}_o + \sin\alpha\vec{r}_e$, where $\vec{r}_o$ and $\vec{r}_e$ depend on the experimental geometry. In our case, $\vec{r}_o = 1/\sqrt{2}[-1,1,0]$ and $\vec{r}_e = 1/\sqrt{2}[-\cos\theta, -\cos\theta, \sqrt{2}\sin\theta]$ (as shown in Fig. 1).

The polarization of the scattered light just after the Raman event is $\vec{e}_s' = R\vec{e}_L'$, with R being the Raman tensor, including the expression in brackets in Eq. (5). As before, $\vec{e}_s'$ is decomposed into its ordinary and extraordinary components, $\vec{e}_s' = \cos\varphi\vec{r}_o + \sin\varphi\vec{r}_e$, with φ being now a function of δ, α, and the tensor parameters. Another $e^{i\delta}$ factor is introduced to account for the phase difference produced as the light goes backward so that the polarization of the scattered light leaving the sample is given by $\vec{e}_s = \cos\varphi e^{i\delta}\vec{r}_o + \sin\varphi\vec{r}_e$. Light in the parallel configuration is obtained by projecting $\vec{e}_s$ onto $\vec{e}_L$, and the intensity in the crossed configuration is found by projecting $\vec{e}_s$ onto a vector perpendicular to $\vec{e}_L$ given by $\vec{e}_\perp = -\sin\alpha\vec{r}_o + \cos\alpha\vec{r}_e$. Then,

$$I_\parallel = C|\vec{e}_L \cdot \vec{e}_s|^2 \quad \text{and} \quad I_\perp = C|\vec{e}_\perp \cdot \vec{e}_s|^2. \tag{7}$$

Applying this method to the nonpolar modes,[22] the dephasing parameters $\delta(\theta)$ for the three planes studied were found: $\delta(001)=0°$; $\delta(111)=45°$; and $\delta(11\frac{1}{2})=47°$ at $\lambda = 514.5$ nm. These values will be taken as fixed parameters in the present work, as they depend only on the medium and crystal orientation but not on each specific mode.

2. Anisotropy of polar modes

For the $\bar{4}$ point group, the Raman tensors of the polar modes are given by

$$B(z) = \begin{pmatrix} c & d & \\ d & -c & \\ & & \end{pmatrix} \quad \text{and} \quad E(x) = \begin{pmatrix} & & e \\ & & f \\ e & f & \end{pmatrix},$$

$$E(-y) = \begin{pmatrix} & & -f \\ & & e \\ -f & e & \end{pmatrix},$$

where the direction of polarization of each type of mode is given in brackets.[11] As shown in Fig. 1, the [−110] direction is contained in all three planes of measurement, thus it is always perpendicular to the phonon propagation direction, as well as to the optic axis $z\|[001]$. These are precisely the conditions for the polarization of an ordinary phonon, so it will be convenient to use another set of matrices for the E modes, one of them representing the ordinary component, with polarization along $y'\|[-110]$, and another one for the extraordinary component, with polarization along $x'\|[110]$. The tensors for E modes are reformulated as

$$E_{\text{extr}} = E(x') = \frac{1}{\sqrt{2}}[E(x) - E(-y)] = \frac{1}{\sqrt{2}}\begin{pmatrix} & & e+f \\ & & f-e \\ e+f & f-e & \end{pmatrix},$$

$$E_{\text{ord}} = E_{\text{TO}} = E(y') = \frac{1}{\sqrt{2}}[E(x) + E(-y)] = \frac{1}{\sqrt{2}}\begin{pmatrix} & & e-f \\ & & e+f \\ e-f & e+f & \end{pmatrix}.$$

For ordinary modes, optical anisotropy affects only the light polarization vectors and their intensity can be calculated as $I(\alpha) = C|\vec{e}_s R \vec{e}_L|^2$, where R is the $E(y')$ tensor:

$$I_\parallel^{E\text{TO}}(\alpha) = C[(f \sin 2\alpha \sin\theta \cos\delta - e \sin^2\alpha \sin 2\theta)^2 + (f \sin 2\alpha \sin\theta \sin\delta)^2], \tag{8a}$$

$$I_\perp^{E\text{TO}}(\alpha) = C[(f \cos 2\alpha \sin\theta \cos\delta - e \sin 2\alpha \sin\theta \cos\theta)^2 + (f \cos 2\alpha \sin\theta \sin\delta)^2]. \tag{8b}$$

As shown in Eq. (5), the intensity of extraordinary modes depends on the phonon propagation and polarization directions. With the geometry of Fig. 1, the propagation direction of the phonon is given by

$$\vec{\kappa} = \frac{1}{\sqrt{2}}(-\sin\theta, -\sin\theta, -\sqrt{2}\cos\theta). \tag{9}$$

We divide the study of Raman intensities of extraordinary modes in the two limiting cases discussed when dealing with phonon frequencies:

(i) When anisotropy forces are stronger than dipolar ones, extraordinary modes correspond to vibrations with polarization either parallel (B type) or perpendicular (E type) to the optic axis, with polarization vectors given by $\boldsymbol{\xi}=[001]$ and $\boldsymbol{\xi}=(1/\sqrt{2})[110]$, respectively. This is the situation fulfilled by modes with $\omega < 230$ cm^{-1}. The negligible or small LO-TO splitting of these modes makes us assume that polarity is weak enough to make $\beta=0$ in Eq. (5) so that the Raman intensity for the extraordinary $\tilde{B}$ modes is given by

$$I(\tilde{B}) = C\left|\sum_{i,j=x,y,z} e_d^i B_{ij}(z) e_L^j\right|^2, \tag{10}$$

and for extraordinary $\tilde{E}$ modes,

$$I(\tilde{E}) = \frac{C}{2}\left|\sum_{i,j=x,y,z} e_d^i [E_{ij}(x) - E_{ij}(-y)] e_L^j\right|^2 = C\left|\sum_{i,j=x,y,z} e_s^i E_{ij}(x') e_L^j\right|^2. \tag{11}$$

Equations (10) and (11) yield that, in this limit, extraordinary modes behave as purely B or E modes with no mixing character. The tensor associated with the extraordinary $\tilde{E}$ mode is $E(x')$, as expected.

Developing Eqs. (10) and (11), the intensities of $\tilde{B}$ modes are given by

$$I_\parallel^{\tilde{B}}(\alpha) = C[(d\cos^2\alpha\cos 2\delta + c \sin 2\alpha \cos\theta\cos\delta - d\sin^2\alpha\cos^2\theta)^2 + (d\cos^2\alpha\sin 2\delta + c\sin 2\alpha\cos\theta\sin\delta)^2], \tag{12a}$$

$$I_\perp^{\tilde{B}} = C[(d\sin\alpha\cos\alpha\cos 2\delta + c\cos 2\alpha\cos\theta\cos\delta + d\sin\alpha\cos\alpha\cos^2\theta)^2 + (d\sin\alpha\cos\alpha\sin 2\delta + c\cos 2\alpha\cos\theta\sin\delta)^2], \tag{12b}$$

and for $\tilde{E}$ modes,

$$I_{\parallel}^{\tilde{E}}(\alpha) = C[(e \sin 2\alpha \sin\theta \cos\delta + f \sin^2\alpha \sin 2\theta)^2 + (e \sin 2\alpha \sin\theta \sin\delta)^2], \quad (13a)$$

$$I_{\perp}^{\tilde{E}}(\alpha) = C[(e \cos 2\alpha \sin\theta \cos\delta + f \sin 2\alpha \sin\theta \cos\theta)^2 + (e \cos 2\alpha \sin\theta \sin\delta)^2]. \quad (13b)$$

(ii) The vibrations of high-frequency modes are quasilongitudinal or quasitransversal. In the $\widetilde{\text{LO}}$ case, $\boldsymbol{\xi} \| \boldsymbol{\kappa}$ so a factor $(1+\beta)^2$ can be taken outside the summation in Eq. (5), which becomes

$$I(\text{LO}) = C(1+\beta)^2 \left| \sum_{i,j=x,y,z} e_d^i [-\sin\theta E(x') - \cos\theta B(z)] e_L^j \right|^2. \quad (14)$$

For $\widetilde{\text{TO}}$ modes we make $\beta=0$ in Eq. (5), since transverse vibrations do not create a dipolar field. For propagation direction $\boldsymbol{\kappa}$ given by Eq. (9), the appropriate polarization vectors for transverse modes are one along [1–10], which corresponds to ordinary modes, already considered, and $\vec{\xi} = 1/\sqrt{2}(-\cos\theta, -\cos\theta, \sqrt{2}\sin\theta)$ for the extraordinary modes. Using this $\boldsymbol{\xi}$, we make the sum over k in Eq. (5) and obtain for $\widetilde{\text{TO}}$ modes

$$I(\text{TO}) = C \left| \sum_{i,j=x,y,z} e_d^i [-\cos\theta E(x') + \sin\theta B(z)] e_L^j \right|^2. \quad (15)$$

Equations (14) and (15) show that $\widetilde{\text{LO}}$ and $\widetilde{\text{TO}}$ extraordinary modes have a mixed B and E character. The mixing depends on the direction of propagation of the modes, given by angle θ from optic axis. For $\theta=0°$, no mixing occurs and Eqs. (14) and (15) become intensities for pure B(LO) and $E(x')$(TO) modes. The contrary happens for $\theta=90°$, where B modes are TO and $E(x')$ are $\widetilde{\text{LO}}$ modes. This behavior coincides with that shown in the discussion of the frequencies.

Developing the treatment of anisotropy of incident and scattered light, we obtain, for $\widetilde{\text{LO}}$modes,

$$I_{\parallel}^{\text{LO}}(\alpha) = C(1+\beta)^2[(e \sin 2\alpha \sin^2\theta \cos\delta + d \cos^2\alpha \cos\theta \cos 2\delta - c \sin 2\alpha \cos^2\theta \cos\delta + f \sin^2\alpha \sin\theta \sin 2\theta + d \sin^2\alpha \cos^3\theta)^2 + (e \sin 2\alpha \sin^2\theta \sin\delta + d \cos^2\alpha \cos\theta \sin 2\delta - c \sin 2\alpha \cos^2\theta \sin\delta)^2], \quad (16a)$$

$$I_{\perp}^{\text{LO}}(\alpha) = C(1+\beta)^2[(e \cos 2\alpha \sin^2\theta \cos\delta - d \sin\alpha \cos\alpha \cos\theta \cos 2\delta - c \cos 2\alpha \cos^2\theta \cos\delta + f \sin 2\alpha \sin^2\theta \cos\theta - d \sin\alpha \cos\alpha \cos^3\theta)^2 + (e \cos 2\alpha \sin^2\theta \sin\delta - d \sin\alpha \cos\alpha \cos\theta \sin 2\delta - c \cos 2\alpha \cos^2\theta \sin\delta)^2], \quad (16b)$$

and, for $\widetilde{\text{TO}}$ modes,

TABLE II. Raman tensor parameters of polar modes in $MnGa_2Se_4$ obtained by fitting equations of $I(\alpha)$ to experimental data.

Approx. $\omega(\text{cm}^{-1})$	Assignment	Tensor parameters
76	$\tilde{E}+E_{\text{TO}}$	nondetermined
93	$\tilde{B}$	$c/d=-2$
105	$\tilde{E}+E_{\text{TO}}$	nondetermined
120–124	$\tilde{B}$	$c/d=0.2$
213–216	$\tilde{E}+E_{\text{TO}}$	nondetermined
225–228	$\tilde{B}$	$c/d=0.1$
237–240	$\widetilde{\text{TO}}+E_{\text{TO}}$	$c/d=0$
243–246	$\widetilde{\text{LO}}$	$e/d=0$; $f/d=-2.5$
252	E_{TO}	$c/d=0$
252–255	$\widetilde{\text{TO}}$	$e/d=0$; $f/d=-0.85$
276–280	$\widetilde{\text{LO}}$	

$$I_{\parallel}^{\text{TO}}(\alpha) = C[(e \sin 2\alpha \sin\theta \cos\theta \cos\delta + d \cos^2\alpha \sin\theta \cos 2\delta + c \sin 2\alpha \sin\theta \cos\theta \cos\delta + f \sin^2\alpha \sin 2\theta \cos\theta + d \sin^2\alpha \sin\theta \cos^2\theta)^2 + (e \sin 2\alpha \sin\theta \cos\theta \sin\delta + d \cos^2\alpha \sin\theta \sin 2\delta + c \sin 2\alpha \sin\theta \cos\theta \sin\delta)^2], \quad (17a)$$

$$I_{\perp}^{\text{TO}}(\alpha) = C[(e \cos 2\alpha \sin\theta \cos\theta \cos\delta + d \sin\alpha \cos\alpha \sin\theta \cos 2\delta + c \cos 2\alpha \sin\theta \cos\theta \cos\delta + f \sin 2\alpha \sin\theta \cos^2\theta + d \sin\alpha \cos\alpha \sin\theta \cos^2\theta)^2 + (e \cos 2\alpha \sin\theta \cos\theta \sin\delta + d \sin\alpha \cos\alpha \sin\theta \sin 2\delta + c \cos 2\alpha \sin\theta \cos\theta \sin\delta)^2]. \quad (17b)$$

Expressions (12a), (12b), (13a), (13b), (16a), (16b), (17a), and (17b) have been used to fit the rotational diagrams $I_{\parallel}(\alpha)$ and $I_{\perp}(\alpha)$ for the (111) and $(11\frac{1}{2})$ planes so as to determine the nature of each peak and the tensor parameters. The usual expressions for isotropic media apply for the (001) plane. Since in this plane only A and B modes are allowed, the assignment is straightforward and gives moreover the c/d relationship for each B mode.

As an example, we show in Fig. 4 the experimental rotational diagrams for the $(11\frac{1}{2})$ plane, as well as the intensities calculated with the parameters indicated in each plot. As can be seen, the angular dependence $I(\alpha)$ is well reproduced except for some very weak modes, whose intensity is difficult to determine. The mode assignments and tensor parameters are given in Table II. Since absolute intensities are not mea-

sured, only relative values of the tensor parameters can be given.

The following restrictions have been applied on performing the fit:

For the low-frequency E modes, the E_{TO} and $\tilde{E}$ components are almost degenerated so that their intensities have been fitted to the sum of Eq. (8a) and (8b) (for the ordinary part) and Eq. (13a) and (13b) (for the $\tilde{E}$ extraordinary part). This sum is proportional to $(e+f)^2$, thus tensor parameters cannot be determined for those modes. On the other hand, the ordinary E_{TO} mode at 240 cm^{-1} is very close to the $\widetilde{\mathrm{TO}}$ quasimode; spectral resolution does not allow us to study both peaks separately so we have fitted the superposition of bands with a sum of Eq. (8a) or (8b) (for the ordinary part) and Eq. (17a) or (17b) (for the $\widetilde{\mathrm{TO}}$ extraordinary part).

At high frequency, each set of E_{TO}, $\widetilde{\mathrm{LO}}$ and $\widetilde{\mathrm{TO}}$ modes must be fitted with the same set of tensor parameters (c,d,e,f) for all three planes, as they are originated from the same B and E modes. It is interesting that for these modes we find the c and e parameters to be zero or negligible, in which case the B and E tensors reduce to

$$B(z)=\begin{pmatrix} & d & \\ d & & \\ & & \end{pmatrix}, \quad E(x)=\begin{pmatrix} & & f \\ & f & \\ & & \end{pmatrix},$$

$$E(-y)=\begin{pmatrix} & & -f \\ & & \\ -f & & \end{pmatrix},$$

which are identified as those of a cubic T_2 mode split into $B+E$ by the tetragonal symmetry. The similarity is not surprising considering that, for the high-frequency modes, the quasicubic assumption is well fulfilled. In fact, the highest-frequency B and E modes are derived from the zone-center mode of zincblende compounds and present similar properties as regards characteristic frequencies, dependence on atomic masses, etc.

In connection with NLO, the most interesting information derived from our work concerns the mechanisms involved in the activity of $\widetilde{\mathrm{LO}}$ modes. The macroscopic field created by longitudinal phonons produces an additional contribution to the Raman intensity, resulting in the appearance of an extra factor $(1+\beta)^2$ in Eqs. (16a) and (16b), as compared to those for the transverse components, Eqs. (17a) and (17b). Thus, β can be determined by comparing the intensities of $\widetilde{\mathrm{LO}}$ and $\widetilde{\mathrm{TO}}$ components within each plane θ. This procedure yields $\beta=-0.2\pm0.1$ for the $\widetilde{\mathrm{LO}}$ mode at 243–246 cm^{-1} and $\beta=1.5\pm0.2$ for the $\widetilde{\mathrm{LO}}$ mode at 276–280 cm^{-1}.

The parameter β is a measure of the relative strength of the field-dependent electro-optic (EO) interaction with respect to the mechanical or deformation potential mechanism, and is directly related to the Faust-Henry coefficient defined for cubic zincblende as[36,37]

$$C_{\mathrm{FH}}=\frac{d_Q}{d_E}\frac{e^*}{\mu}\frac{1}{\omega_{\mathrm{TO}}^2},$$

where $d_Q=\partial\chi/\partial Q$ and $d_E=\partial\chi/\partial E$, χ is the dielectric susceptibility, Q represents a phonon coordinate, E the component of the macroscopic electric field along $\boldsymbol{q}_{\mathrm{LO}}$, e^* is the effective charge of the mode, and μ is its effective mass ($\mu^{-1}=m_A^{-1}+m_B^{-1}$ for the zone-center mode of an AB zincblende compound).[37] With the equivalence $\beta=(d_E/d_Q)(\mu/e^*)(\omega_{\mathrm{TO}}^2-\omega_{\mathrm{LO}}^2)$,[38] we have

$$C_{\mathrm{FH}}=\frac{1}{\beta}\frac{\omega_{\mathrm{TO}}^2-\omega_{\mathrm{LO}}^2}{\omega_{\mathrm{TO}}^2}.$$

Taking the value $\beta=1.5$ for the highest frequency, pseudocubic mode, and the phonon frequencies $\omega_{\mathrm{TO}}=255$ cm^{-1} and $\omega_{\mathrm{LO}}=280$ cm^{-1}, we obtain $C_{\mathrm{FH}}=-0.14$, which is of the same order of magnitude as in II–VI cubic analogs.[37] Conversely, by taking the C_{FH} constants listed in Ref. 37 and TO, LO frequencies from the literature, we can use the relation between β and C_{FH} to derive the value of β for related II–VI compounds: $\beta=3.24$ for ZnS, 2.95 for ZnTe, and either 0.6 or ≈2 for ZnSe, depending on the C_{FH} used for this compound. The relation between β and the EO and nonlinear coefficients can be found in Refs. 9 and 10.

V. CONCLUSIONS

We have studied the Raman spectrum of $MnGa_2Se_4$ regarding effects derived from its structural anisotropy. Uniaxial optical behavior leads to dephasing between ordinary and extraordinary component of light and modifies the selection rules of polar and nonpolar modes. The influence of anisotropy in polar modes yields a mixed E/B or LO/TO character, except in high-symmetry planes. For a correct interpretation of the spectrum, the Loudon equations for the frequencies and for the intensities must be applied. A detailed study of the intensities of polar modes allows us to determine the strength of local dipolar electric fields. The determination of these properties may be of interest for the optoelectronic applications of this material.

ACKNOWLEDGMENT

This work was performed with financial support from the Spanish Ministry of Education and Science under Project No. MAT2007-64486-C07-02.

*sanjuan@unizar.es

[1] S. Adachi, *Properties of Group-IV, III-V and II-VI Semiconductors*, Wiley Series in Materials for Electronic and Optoelectronic Applications (Wiley, New York, 2005); V. G. Dimitriev, G. G. Gurzadyan, and D. N. Nikogosyan, *Handbook of Nonlinear Optical Crystals*, 2nd ed. (Springer, New York, 1997).

[2] L. K. Samanta, D. K. Ghosh, and G. C. Bhar, Phys. Rev. B **33**, 4145 (1986).

[3] M. C. Ohmer, R. Pandey, and N. H. Baraimov, MRS Bull. **23**, 16 (1998).

[4] L. Isaenko, A. Yelisseyev, S. Lobanov, P. Krinitsin, V. Petrov, and J.-J. Zondy, J. Non-Cryst. Solids **352**, 2439 (2006).

[5] A. N. Georgobiani, S. I. Radautsan, and I. M. Tiginyanu, Sov. Phys. Semicond. **19**, 121 (1985).

[6] L. K. Samanta, D. K. Ghosh, and P. S. Ghosh, Phys. Rev. B **39**, 10261 (1989).

[7] V. Petrov and F. Rotermund, Opt. Lett. **27**, 1705 (2002).

[8] B. F. Levine, C. G. Bethea, and H. M. Kasper, IEEE J. Quantum Electron. **10**, 904 (1974); B. F. Levine, C. G. Bethea, H. M. Kasper, and F. A. Thiel, *ibid.* **12**, 367 (1976).

[9] W. Hayes and R. Loudon, *Scattering of Light by Crystals* (Wiley, New York, 1978).

[10] W. D. Johnston and I. P. Kaminow, Phys. Rev. **188**, 1209 (1969); W. S. Otaguro, E. Wiener-Avnear, and S. P. S. Porto, Appl. Phys. Lett. **18**, 499 (1971).

[11] R. Loudon, Adv. Phys. **13**, 423 (1964).

[12] T. C. Damen, S. P. S. Porto, and B. Tell, Phys. Rev. **142**, 570 (1966).

[13] C. A. Arguello, D. L. Rousseau, and S. P. S. Porto, Phys. Rev. **181**, 1351 (1969).

[14] R. F. Schaufele and M. J. Weber, Phys. Rev. **152**, 705 (1966).

[15] C. Razzetti, P. P. Lottici, and R. Bacewicz, J. Phys. C **15**, 5657 (1982).

[16] N. N. Syrbu, L. L. Nemerenco, and O. Cojocaru, Cryst. Res. Technol. **37**, 101 (2002).

[17] A. Eifler, J.-D. Hecht, V. Riede, G. Lippold, W. Schmitz, G. Krauß, V. Krämer, and W. Grill, J. Phys.: Condens. Matter **11**, 4821 (1999).

[18] A. Miller, A. Mackinnon, and D. Weaire, Solid State Phys. **36**, 119 (1981).

[19] M. Cannas, L. Garbato, A. G. Lehmann, N. Lampis, and F. Ledda, Cryst. Res. Technol. **33**, 417 (1998).

[20] H. Haeuseler, J. Solid State Chem. **26**, 367 (1978).

[21] M. L. Sanjuán and M. C. Morón, Physica B **316-317C**, 565 (2002).

[22] P. Alonso-Gutiérrez, M. L. Sanjuán, and M. C. Morón, Phys. Rev. B **71**, 085205 (2005).

[23] F. Leccabue, B. E. Watts, C. Pelosi, D. Fiorani, A. M. Testa, A. Pajaczkowska, G. Bocelli, and G. Calestani, J. Cryst. Growth **128**, 859 (1993).

[24] M. C. Morón and S. Hull, Phys. Rev. B **64**, 220402(R) (2001).

[25] A. Millán and M. C. Morón, J. Appl. Phys. **89**, 1687 (2001).

[26] P. Alonso-Gutiérrez, M. L. Sanjuán, and M. C. Morón, *Proceedings of the 28th International Conference on the Physics of Semiconductors*, AIP Conf. Proc. No. 893 (AIP, New York, 2007), p. 185.

[27] P. Alonso-Gutiérrez and M. L. Sanjuán, Phys. Rev. B **76**, 165203 (2007).

[28] O. Brafman and S. S. Mitra, Phys. Rev. **171**, 931 (1968).

[29] R. C. C. Leite, T. C. Damen, and J. F. Scott, in *Light Scattering Spectra of Solids*, edited by G. B. Wright (Springer, New York, 1969).

[30] J. González, B. J. Fernandez, J. M. Besson, M. Gauthier, and A. Polian, Phys. Rev. B **46**, 15092 (1992).

[31] A. M. Andriesh, N. N. Syrbu, M. S. Iovu, V. E. Tazlavan, Phys. Status Solidi B **187**, 83 (1995).

[32] J. F. Scott and S. P. S. Porto, Phys. Rev. **161**, 903 (1967).

[33] P. Brüesch, *Phonons: Theory and Experiments I*, Springer Series in Solid-State Sciences Vol. 34, edited by M. Cardona, P. Fulde, and H.-J. Queisser (Springer, Berlin, 1982), p. 126.

[34] The parameter α introduced by Loudon as a prefactor to ζ^k was here assumed to be integrated into the Raman tensor elements, so that, in fact, our β is equivalent to Loudon's β/α.

[35] M. Born and E. Wolf, *Principles of Optics* (Pergamon, New York, 1975).

[36] W. L. Faust and C. H. Henry, Phys. Rev. Lett. **17**, 1265 (1966).

[37] M. Cardona, in *Light Scattering in Solids II*, Topics in Applied Physics Vol. 50, edited by M. Cardona and G. Guntherodt (Springer, New York, 1982), Chap. 2.

[38] Strictly speaking, there may be two different β constants, related to B_{LO} and E_{LO} modes, respectively, but since high-frequency modes behave as quasicubic ones, we shall assume that a single β exists for each (B,E) pair and that it takes the cubic value.